Geophys. J. Int. (2009) **179,** 489–499 doi: 10.1111/j.1365-246X.2009.04303.x

Seismicity patterns and variation of the frequency-magnitude distribution of microcracks in salt

Nina Köhler,[1,*] Thomas Spies[2] and Torsten Dahm[1]

[1] *Institute of Geophysics, University of Hamburg, Hamburg, Germany. E-mail: nina.koehler@gpi.uni-karlsruhe.de*
[2] *Federal Institute for Geosciences and Natural Resources (BGR), Hanover, Germany*

Accepted 2009 June 18. Received 2009 June 18; in original form 2008 September 8

SUMMARY

We analyse the statistical behaviour of about 1.6 E+6 high-frequency, acoustic emission events recorded in a rock mass in a salt mine over a 3-yr time period. The rock mass is directly located above a cavity that is backfilled during a 6 months time interval within the investigated time period. The rock mass consists mainly of rock salt with large anhydrite blocks in it. Location, event rate and strength of the events are studied in 3 months time intervals before, during, and after the backfilling process. We observe strong temporal and spatial changes of event rate and *b*-values that correlate with the structural features and the loading of the rock mass: two regions with a *b*-value maximum above the cavity start developing with the beginning of backfilling. They reach extremely high *b*-values of up to $b = 3.18$ and are located at the transition zones between the different materials. The *b*-value ratio in anhydrite and rock salt anti-correlates during times of equilibrium and fast loading. We conclude that *b*-value mapping during transient loading is useful to investigate structural heterogeneities in the rock volume, whereas *b*-values during equilibrium phases better indicate the level of ambient stress and visco-plastic stress relaxation in the salt rock.

Key words: Earthquake interaction; Seismicity and tectonics; Statistical seismology.

INTRODUCTION

In this study, the spatial and temporal variations of the frequency-magnitude distribution, the so-called *b*-value, were derived from acoustic emission (AE) data in the Morsleben salt mine in eastern Germany. The work was motivated by the extremely high number of AE events that were located in the investigated rock mass above a cavity that has been backfilled during the study period. The Morsleben salt mine (Fig. 1) is located in the Allertal zone, a 4–5 km wide and about 50 km long, NW–SE-oriented fault (Federal Office for Radiation Protection 2001). The embedded Zechstein salt body is primarily a tectonic structure, resulting from Late Cretaceous compression within the North German basin (Behlau & Mingerzahn 2001). It has a thickness between 380 and 500 m (Kreienmeyer *et al.* 2004) and is covered by an up to 200 m thick layer of cap rock. The salt structure encloses many blocks of anhydrite, but there are also parts of potash salt in it. The layers show multiple folds with mainly horizontal axes oriented NW–SE, that is parallel to the trend of the Allertal zone (Behlau & Mingerzahn 2001).

The Morsleben salt mine has a length of 5.6 km and an average width of 1.4 km (Fig. 1). Its four main levels reach down to a depth of 500 m below sea level. Until 1969, the Morsleben salt mine was mainly used for mining of potash and rock salt. During mining, large excavation sites in form of cavities were built, showing typical dimensions of 100 m length, 30 m width and 30 m height. This led to a total cavity volume of 5.8 million m^3 (Federal Office for Radiation Protection 2001).

Within the rock masses close to the cavities, deformation occurs that lead to a development of microcracks with dimensions of millimetres to centimetres. They are associated with dilatancy, that is the irreversible volume increase of the rock mass. It results likewise in an increase of the rock permeability (Spies & Eisenblätter 2001b; Spies *et al.* 2005). During these microcracking processes, AE, that is high-frequent elastic energy, is emitted. The AE monitoring is used as an indicator for microcracking and allows drawing conclusions about the stability of the cavity system.

The frequency-magnitude relation is defined as

$$\log N = a - bM, \tag{1}$$

where N is the number of events showing a magnitude of M or larger (e.g. Ishimoto & Iida 1939; Gutenberg & Richter 1949). The parameters a and b are constants. The parameter b is the slope of the distribution and is typically $b = 1.0$, whereas a measures the number of events with given b and $M_{\min}$ (Wyss 1973). The relation relies on the observation that the number of smaller events in a seismic catalogue is considerably higher than the number of large events.

*Now at: Geophysical Institute, University of Karlsruhe, Karlsruhe, Germany.

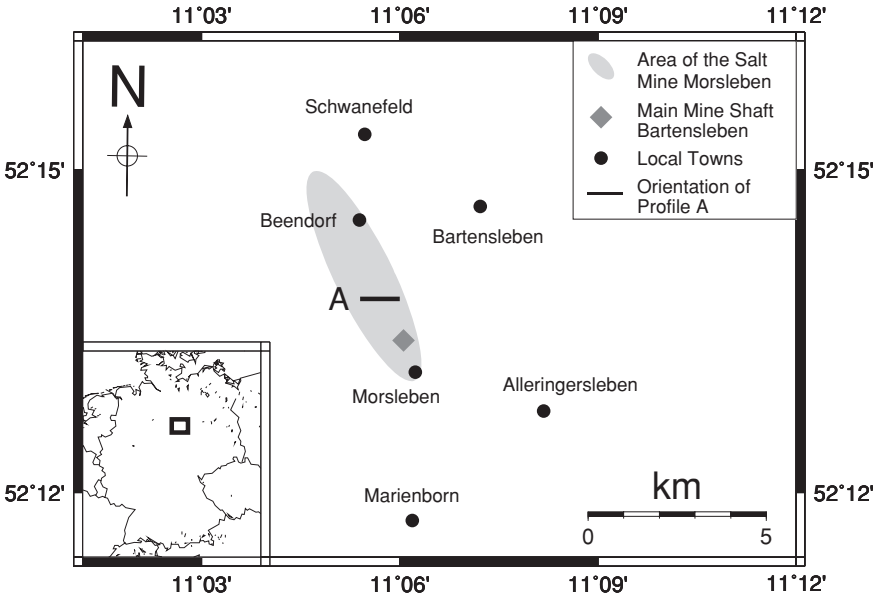

Figure 1. Sketch of experimental site. The location of the Morsleben salt mine is indicated as a grey ellipse. The profile A, indicated by a solid line, represents the location of the later described cross-section. For a better overview, the length of the profile is exaggerated by a factor of 11.

The AE events in our study are assumed to have small-scale source mechanisms similar to earthquakes on large scale (Spies *et al.* 2005). The analysis of the frequency-magnitude distribution led to unusually high *b*-values of up to 3.18.

Indeed, different authors showed that the frequency-magnitude relation holds not only for earthquakes but also for microfractures (Mogi 1962; Scholz 1968). By performing rock deformation experiments in the laboratory, Mogi (1962) and Scholz (1968) each suggested a different meaning of the frequency-magnitude distribution of microfractures. Mogi (1962) proposed that *b* increases with the degree of heterogeneity and by an increase of the crack density with time. Scholz (1968), however, found that *b* depends primarily on stress rather than on the heterogeneity of the material. He observed that *b* decreases with an increase of shear stress or with a decrease of the confining pressure. From this he inferred that, as stress is increased, the events become statistically larger. Scholz (1968) also observed that *b* is much higher for frictional sliding and deformation of a ductile rock than for brittle rock. He explained this with large sudden stress drops that occur during frictional sliding of brittle rock under high confining pressure.

Recent studies indicated the inverse relationship between the *b*-value and the stress and showed its consistency with further laboratory experiments (e.g. Amitrano 2003) or with induced seismicity during mining (Urbancic *et al.* 1992). Schorlemmer *et al.* (2005) proposed that *b* acts as a stressmeter that depends inversely on differential stress. They observed that *b* is highest for normal faulting events, lowest for thrust events and intermediate for strike-slip events, assuming that thrust faults tend to be under higher stress than normal faults. By arguing that differential stress is tied to confining pressure, Schorlemmer *et al.* (2005) inferred from this that the inverse relationship between the *b*-value and the differential stress is universally valid, ranging from sub-millimetres to hundreds of kilometres of rupture length.

Further previous studies have revealed that the size of the *b*-value is not necessarily limited to values between 0 and 1.0. For example, volcanic areas often showed *b*-values greater than 1.3 (Wiemer & McNutt 1997), whereas thermal experiments in the laboratory led to *b*-values of up to 2.7 (Warren & Latham 1970). The authors concluded that these higher values were due to fracturing produced by thermal stresses, whereas three main factors were proposed to have significant effects on the *b*-value: the tendency towards the formation of a systematic fracture pattern, the inhomogeneity of the material and the spatial variations in the temperature distribution within the material (Warren & Latham 1970).

For AE experiments, information about the behaviour of the frequency-magnitude distribution is only sparse. However, AE monitoring of the Äspö Pillar Stability Experiment at the Hard Rock Laboratory of the Swedish Nuclear Fuel and Waste Management Co (SKB) in Sweden gave a *b*-value of 4.4 (Haycox *et al.* 2005). In the experiment, a pillar between two boreholes in a waste repository was monitored. The aim of the experiment was to demonstrate the effect of backfill and confining pressure on the propagation of microcracks in rock adjacent to deposition holes. According to the authors, this high *b*-value is similar to *b*-values recorded in other high-frequency AE experiments (Hazzard 1998; Pettitt 1998). For example, Hazzard (1998) used dynamic geomechanical models to investigate brittle failure and dynamic behaviour of rocks and the resulting synthetic acoustic output. The axially loading of a granite model led to a *b*-value of about 5.5, whereas each bond breakage between the individual particles of the granite model was considered as a single seismic event. Hazzard (1998) discovered that *b*-values in the order of 1.0 could only be gained by clustering some of the bond breakages into larger seismic events.

DATA AND METHOD

The AE events used for this study were recorded by a network of 24 piezoelectric sensors in the frequency range of 1–100 kHz. For comparison, microseismic studies are usually performed in the frequency range of about 20 Hz to about 10 kHz (Spies *et al.* 2005). The sensors are installed in boreholes that are drilled from the cavities.

The locations of the AE events were determined automatically on site by inversion of the traveltimes of *P* and *S* waves. The

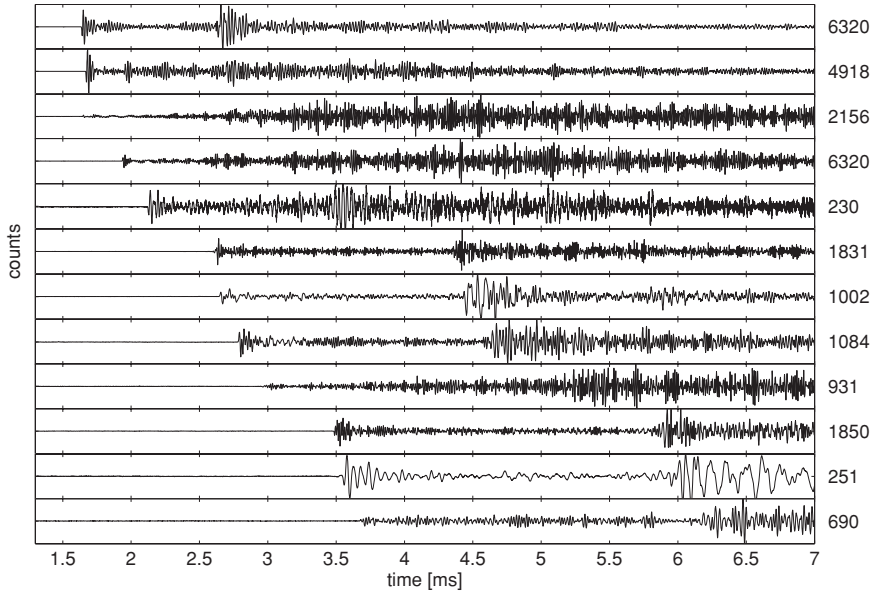

Figure 2. Raw data example of a typical AE event from the Morsleben salt mine, recorded at 12 sensors of the seismic network. The records are sorted over distance and scaled at their maximum amplitudes that are given on the right-hand side (in counts).

P-wave onsets were automatically picked using only signals with high signal-to-noise ratio (greater 10). These were used for a first estimation of the source coordinates by an iterative least squares procedure. If the residuals were larger than 0.18 ms (eqiuvalent to 0.8 m), the onsets with the largest residuals were stepwise eliminated and new solutions were calculated until the residuals fell below the 0.18 ms limit. Additionally, the *S*-wave onsets were automatically picked within the time intervals that were expected by the localization results using *P* waves only. The respective threshold for the *S*-wave onsets is 0.31 ms (equivalent to 0.8 m). *P*- and *S*-wave onsets with large residuals were again eliminated until the error fell below the threshold. Locations were only considered as valid if at least ten onsets of *P* or *S* wave remained (Spies *et al.* 2005). The obtained localization accuracy is 3 m or less. A typical example of a recorded event can be found in Fig. 2.

The size of the events was determined analogue to the magnitude in seismology by using the maximum amplitudes of the 24 sensor signals and the distances from the AE sources to the sensors. The mean amplitude is defined as the amplitude value of the linear regression curve at a reference distance of 50 m from the source, as seen in Fig. 3. This AE magnitude M_{AE} is specified in dB with a reference voltage of 1 μV prior to amplification (Spies & Eisenblätter 2001a,b; Spies *et al.* 2005). The magnitudes of the AE events investigated in this study range between 1.5 and 157.8 dB. Fig. 3 shows an example of the magnitude determination for an event of $M_{\mathrm{AE}} = 48.2$ dB.

The frequency-magnitude distribution

To ensure the stability of the central part of the mine, 20 cavities were chosen to be backfilled with a salt concrete. Although backfilling will also cause temporal additional loads such as a rise of temperature or moisture due to the setting of the concrete, it is still expected that ongoing dilatancy will decrease in the long term and the positive effects of the procedure will be dominant (Spies *et al.* 2005).

In this work, we investigate the effect of backfilling of the first cavity on the AE event rate, on the seismicity patterns, and on the frequency-magnitude distribution in the vicinity of the cavity. The investigated cavity and its location relative to the sensor network are displayed in Fig. 4. The cavity is located at a depth of –310 m below sea level and is of 90 m length, 30 m width and 12 m height. The cavity covers a volume of about 25 500 m^3. All coordinates used in this study are Gauss-Krueger coordinates. The backfilling of the cavity started at the end of September 2003 and ended at the beginning of April 2004.

The cure of the concrete led to a release of heat and moisture to the surrounding rock mass. This additional load caused an increase of the number of microcracks and therefore an increase of the number of located events. As an example of the seismicity distribution, AE events in the magnitude ranges 70 to 72 dB and 80 to 82 dB are plotted in Fig. 4. The large rectangle in Fig. 4 indicates the region where most of the recorded and in this study investigated AE events are located. This rock mass is situated right above the cavity and has a thickness of 100 m. As obvious from Fig. 4, the network coverage for the rock mass is not uniform; the main part of the network is located outside of the investigated area. Fig. 5 displays the temporal development of the daily frequency of located events during the investigated time interval of 3 yr, that is 21 months before backfilling started until 9 months after backfilling was finished. Due to maintenance or failures of the network, some short temporal gaps exist in the catalogue. In the time period before backfilling started, the number of located AE events varies between 163 and 990 events per day. Within the first 2 months of backfilling, the daily number increases up to 4297 events. For the remaining time of the backfilling period, the numbers show a decreasing tendency. Shortly after backfilling is finished, the daily number rapidly increases again to a maximum value of 5907 events during the next 3.5 months, but then shows a decreasing trend for almost the rest of the investigated time period. From December 24, 2004, to the end of the year, the rate of located events increases again due to stopping of working in the mine. The black curve in Fig. 5 shows the temperature measured at the ceiling of the cavity during and after the backfilling process. The emitted

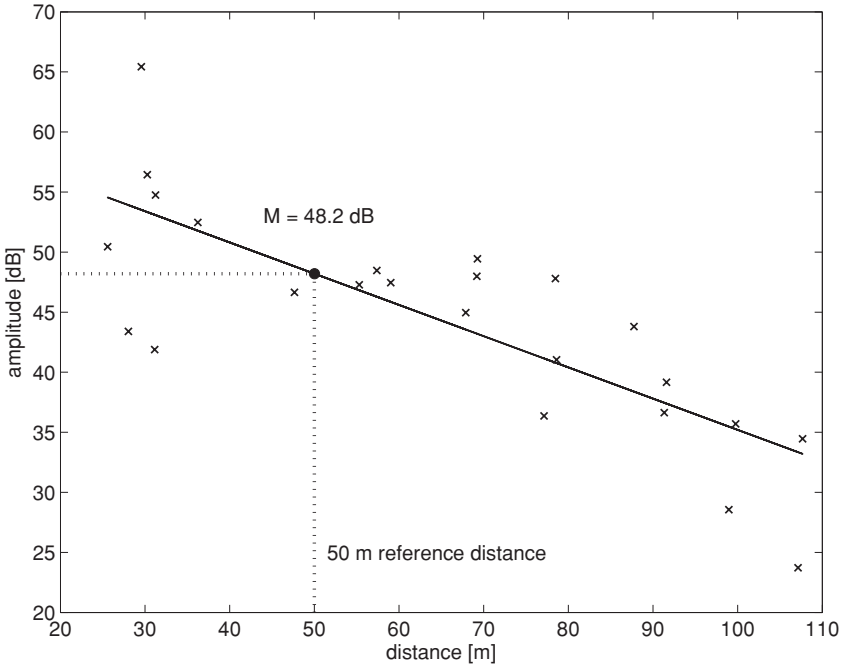

Figure 3. Example of amplitude attenuation with distance for an acoustic event from 2002 December 15, recorded at all 24 sensors (black crosses). Specific station correction factors are subtracted from the measured amplitude values. The event magnitude $M_{\mathrm{AE}} = 48.2$ dB was determined by the amplitude value of the linear regression curve at a reference distance of 50 m. The slope of the regression line represents the damping coefficient of –0.26 dB m^{-1}.

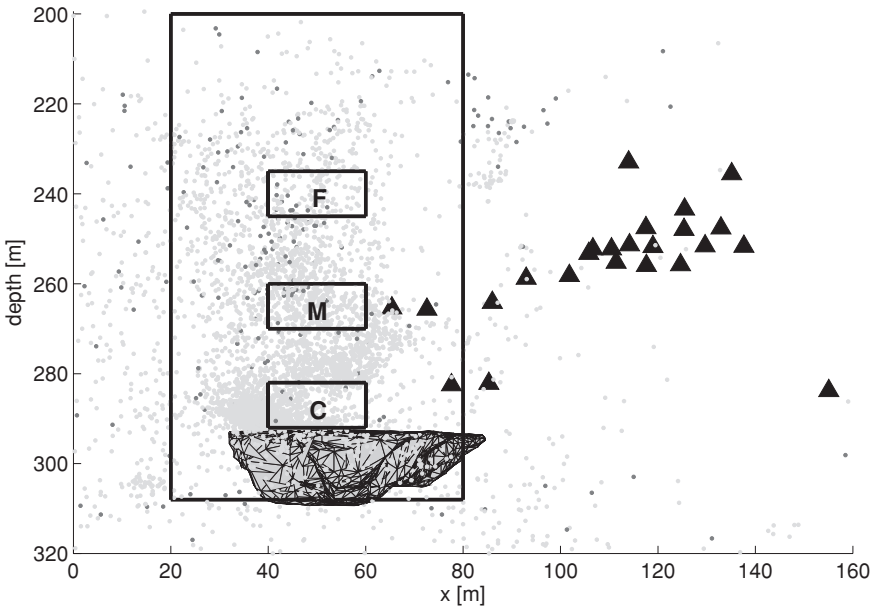

Figure 4. Vertical section of profile A. The polygon shows the backfilled cavity, the triangles indicate the projected positions of the borehole sensors of the network. The light grey dots show the locations of all AE events in a magnitude range between 70 and 72 dB, and the dark grey dots give the locations of all events between 80 and 82 dB. The large rectangular box gives the region from where AE events were used for this study. The smaller solid boxes indicate the three regions (C: close, M: middle, F: far away from the cavity) from which AE events were taken for a more detailed investigation.

heat due to the setting of the concrete leads to a strong temperature increase within the rock around the cavity. The temperature increases by 42 °C during the time of backfilling. The rhythm between weekdays and weekends, where backfilling was stopped, is clearly visible.

The rapid increases of the AE rate are due to the strong temperature variations that induce changes of stress in the rock, not only during backfilling, but especially afterwards when the temperature cools down again.

For investigating the frequency-magnitude distribution of our catalogue, we use ZMAP 6.0, a software package for analysing seismicity (Wiemer 2001). All following results on *b*-values and magnitude of completeness (M_c) were calculated using the software. Fig. 6 shows the frequency-magnitude distribution of the overall

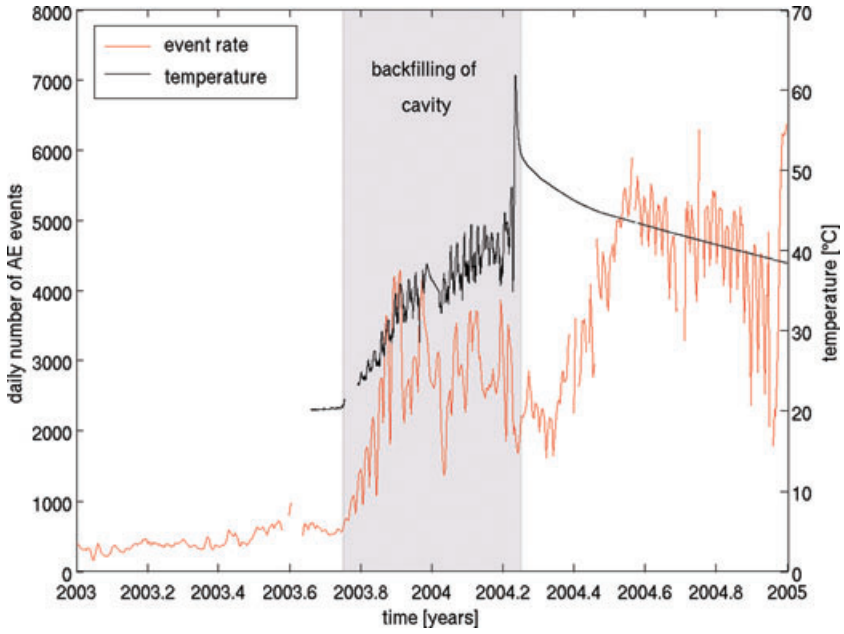

Figure 5. The total occurrence rate of AE events (red curve) in the investigated rock volume and the temperature variations (black curve) measured above the ceiling of the cavity are plotted versus time. The time series have been smoothed using a moving average filter with a span of 5 days. The grey-filled area declares the time period of backfilling of the cavity.

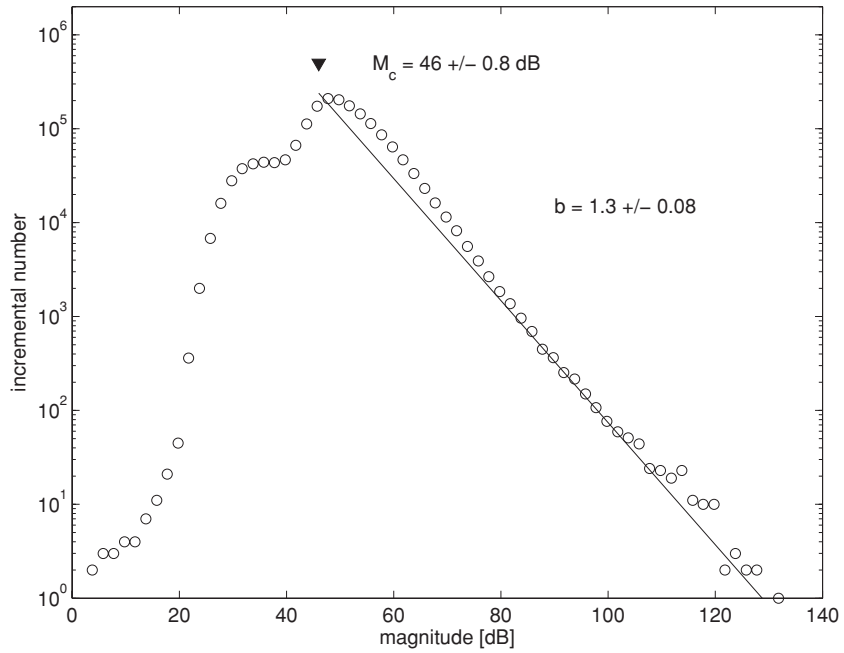

Figure 6. Frequency-magnitude distribution of the overall dataset used in this study. The dataset is cut at 130 dB to avoid influence from a potential saturation of the seismic network. The line shows the manually determined slope of the incomplete part of the distribution, using an automatically determined magnitude of completeness.

dataset used in this study. The dataset is cut at 130 dB to avoid influence from a potential saturation of the seismic network. This means that we excluded two events, one with 138 dB and one with 158 dB. A magnitude of completeness of 46 ± 0.8 dB is obtained by using the automatic entire magnitude range (EMR) method of ZMAP 6.0 together with a bootstrapping technique (100 bootstraps) for estimating the uncertainties (Schorlemmer *et al.* 2003). The EMR method is a robust estimation method that also uses the events with smaller magnitudes than M_c. It applies a maximum-likelihood (Aki 1965) estimator for a model that consists of two parts: one to model the complete part, and one to sample the incomplete part of the frequency-magnitude distribution (Woessner & Wiemer 2005). We then used this M_c to determine a b-value of 1.3 ± 0.08 by manually selecting the starting and ending magnitude values. This

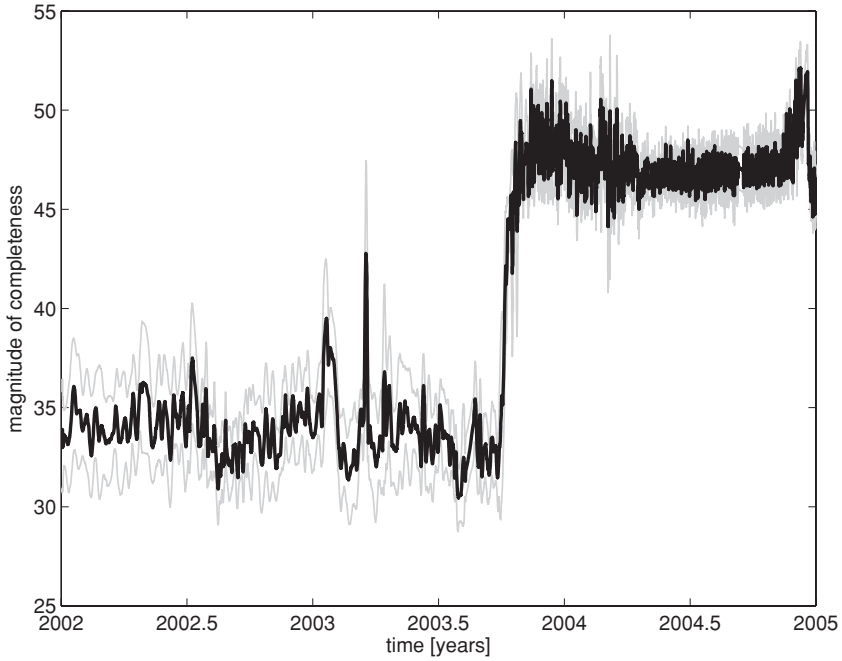

Figure 7. Magnitude of completeness with time of the overall dataset used in this study (black curve) and its uncertainties (grey curves).

b-value is larger than the general assumed value of 1.0, because it averages both regions and time periods showing smaller and much higher *b*-values than 1.0.

However, M_c varies with time (Fig. 7): for the time period before backfilling started, M_c has an average value of 33.7 dB. With the beginning of backfilling, it increases to an average of 47.1 dB. M_c is again calculated using the EMR bootstrapping technique (100 bootstraps). The sudden increase in M_c is caused by the starting backfilling activity. The background noise and the overall increase of seismicity overlay the smallest events. The spatial variation of M_c in the region of main interest, that is above the cavity, is 5 per cent or less, and can reach similar values than the temporal variations of M_c in the border region of the area.

Fig. 8 shows the event rate per night over the whole time period for the three sub-volumes indicated in Fig. 4. The 5, 25 and 50 m curves show the event rates for all events located in the sub-volumes C, M and F, respectively. The grey marked time period marks the backfilling process, which was stopped over the Christmas break in 2003.

The vertical grey lines represent weekend days at which backfilling was stopped. At the end of the investigated time period (yr 2004.68 to 2004.96), another cavity further away was backfilled as well. Again, it can be clearly seen that at times at which backfilling rested—especially right after the end of backfilling—the event rate increases drastically due to the temperature changes. Additionally, it can be observed that the mean event rate not only increases some time after the end of backfilling and stays at this level, but also that this increase is time shifted for the three sub-volumes: the earliest increase takes place at the furthest distance to the cavity, the latest increase close to the cavity. The backfilling primarily seems to have an effect on some remote parts of the rock mass.

Fig. 9 displays the temporal and spatial variations in the event density within a 2-D cross-section through the investigated rock mass before, during, and after backfilling. Main parts of the seismicity concentrate on smaller areas, whereas the regions further outside only show a much less event density or no seismicity at all. As soon as backfilling starts, the events start clustering above the roof of the cavity (Figs 9b–f). A second area with remarkably high event density develops about 50 m above the cavity, at a depth of –240 m.

For investigating both the spatial and temporal variations of the *b*-values, we calculate a 3-D frequency-magnitude distribution. To do so, a 3-D grid was defined through the investigated rock mass above the cavity with cubic grid cells of each 4 m edge length. We applied two different approaches: the *b*-values were both calculated using a constant number of events per grid cell as well as a constant radius around each grid node. Using the first method, the algorithm continues searching for events in the area around the specific element until the pre-defined number of events has been found. The second method uses all events that are located in the given volume. The *b*-values are automatically calculated at each grid node using only events from the subsets that are larger than the magnitude of completeness. M_c is estimated at each grid node automatically by applying the maximum curvature method of ZMAP 6.0 (Wiemer & Wyss 2000; Woessner & Wiemer 2005).

Although the method of constant number of events guaranties a more constant accuracy of *b,* the spatial resolution is less reliable compared to the method of constant radius. However, the results presented in this work are obtained by using the method of constant event numbers. Comparisons between the two methods did not lead to significant changes neither in the size of *b*-values nor in their spatial distributions.

Fig. 10 shows the results of the frequency-magnitude distribution throughout the different time steps of the study period. Displayed is the same cross-section than in Fig. 9. For the time period before backfilling started (Fig. 10a), the *b*-values were calculated using 100 events per grid cell. For the later time periods (Figs 10b–f), 1000 events per grid cell were used due to the higher event density. Note that the colour scale of the *b*-values is clipped at 2.5 for better resolution.

Before backfilling started, the rock mass above the cavity shows *b*-values in the range of 0.7–2.2, whereas the higher *b*-values

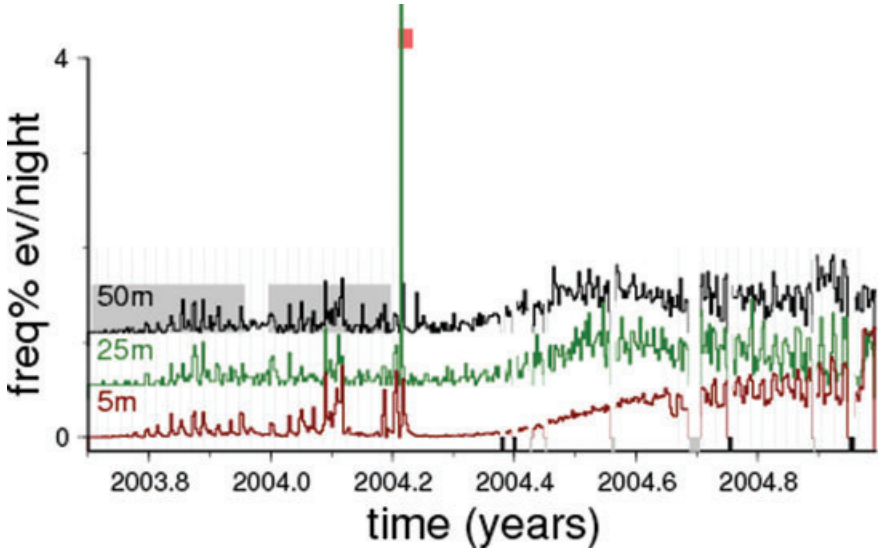

Figure 8. Event rate per night over the whole time period for the three sub-volumes indicated in Fig. 4. The 5, 25 and 50 m curves show the event rates for all events located in the sub-volumes C, M and F, respectively. The grey marked time period marks the backfilling process, which was stopped over the Christmas break in 2003. The vertical grey lines represent weekend days at which backfilling was stopped. At the end of the investigated time period (yr 2004.68 to 2004.96), another cavity further away was backfilled as well. The temporal gaps in the event rate are marked by small grey bars.

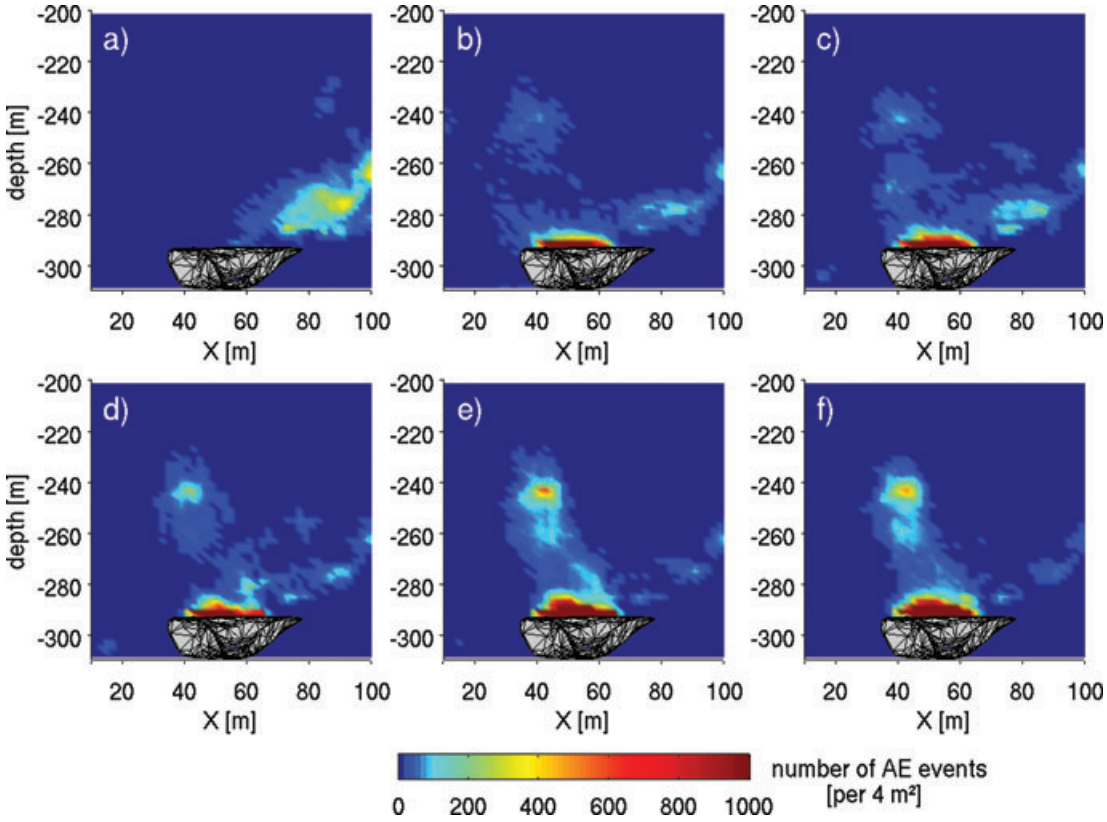

Figure 9. Areal AE event density of events projected on the vertical profile A during different time periods from (a) January 2002 to September 2003, (b) October to December 2003, (c) January to March 2004, (d) April to June 2004, (e) July to September 2004 and (f) October to December 2004. The orthogonal range of projection is ±15 m. The colour scale indicates the number of projected AE events per 4 m^2 and is clipped at 1000 events.

concentrate on two depths of about –235 and –275 m, respectively (Fig. 10a). However, due to the small number of registered events (Fig. 9a), the *b*-value results from this time period need to be considered with caution. During backfilling (Figs 10b and c), the area of higher *b*-values at a depth of –235 m enlarges to an eastwards ascending structure with *b*-values between 2.0 and 2.1. When backfilling was finished, this area enlarges again to a kidney-shaped volume of high *b*-values that reach from about –210 m depth down to almost the roof of the cavity. In its centre around –240 m depth, the *b*-values are highest and reach their maximum value of $b = 3.18$ during

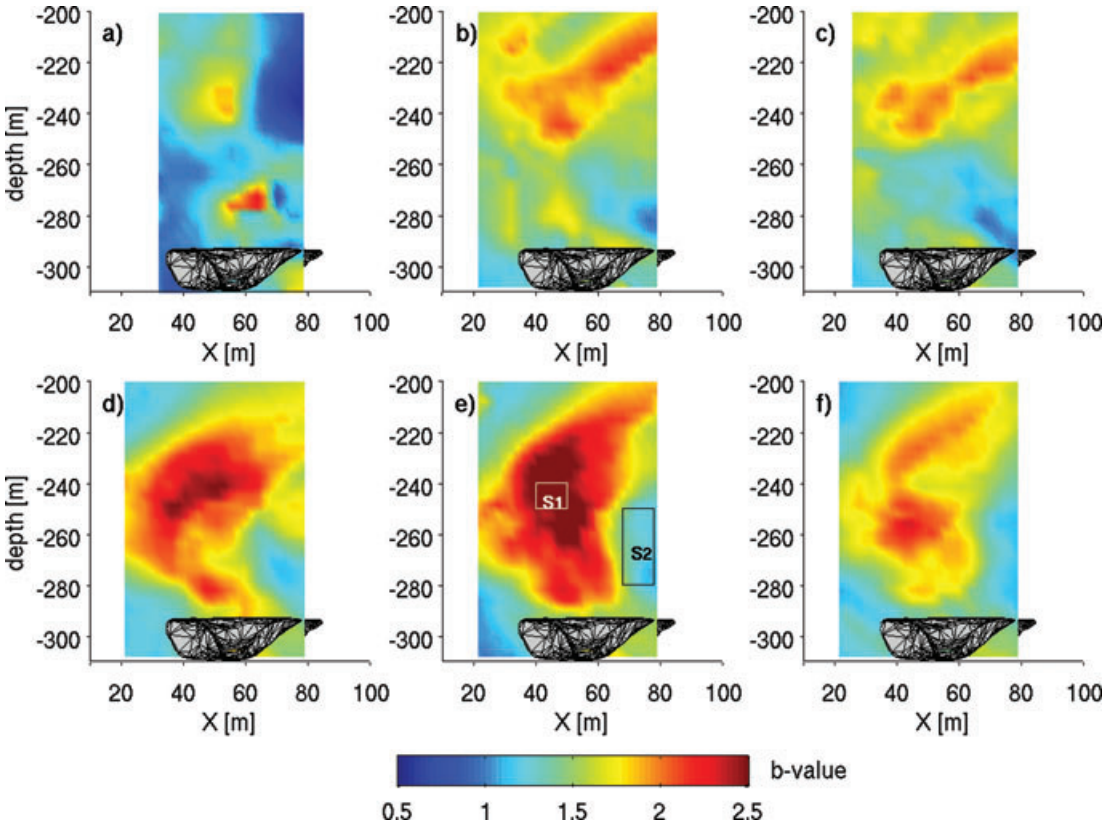

Figure 10. *b*-values along profile A associated with cubes of variable size, each containing 100 (a) and 1000 (b–f) events, respectively. The time intervals (a–f) are the same than for Fig. 9. The colour scale indicates the *b*-values and is clipped at 2.5. S1 and S2 show the locations of the two subsets of AE events from that the frequency-magnitude distributions presented in Fig. 11 are derived.

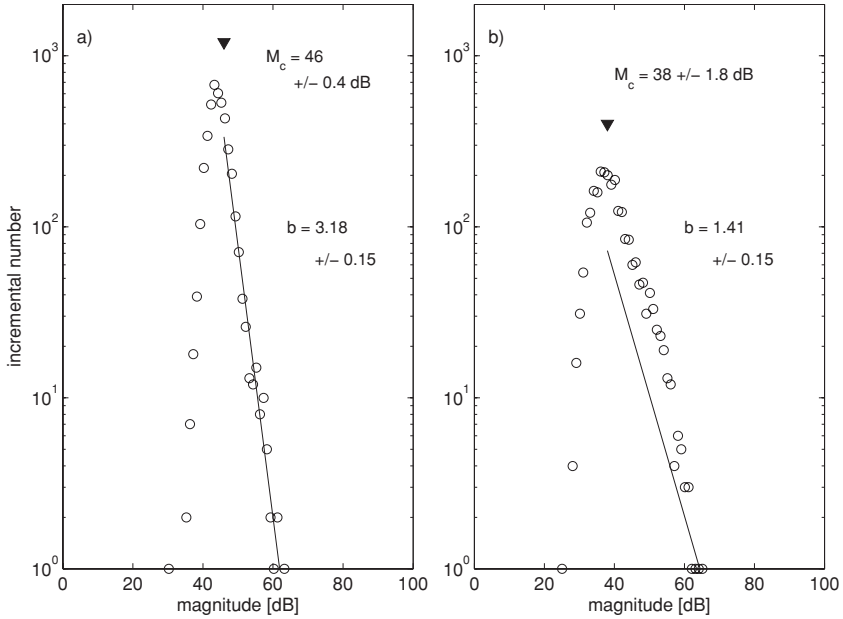

Figure 11. Frequency-magnitude distributions of the AE events located in the subsets S1 (a) and S2 (b) in Fig. 10. The inverted triangles indicate the magnitudes of completeness, and the lines show the automatically determined slopes of the incomplete parts of the distributions.

the time period 3 months after backfilling was finished (Fig. 10e). The outer parts of the investigated area have *b*-values of about 1.0–1.4, showing a narrow transition zone to the kidney-shaped volume. Fig. 11 shows the individual frequency-magnitude distributions derived from the two regions S1 and S2 as indicated in Fig. 10(e). The *b*- and M_c-values are determined using the EMR method together with the bootstrapping technique (100 bootstraps). They show clearly the difference in *b* between these two subsets.

During the last 3 months of the study period (Fig. 10f), the *b*-values decrease to values between 1.6 and 2.3 within the kidney-shaped volume that is still clearly visible.

The standard deviation of the *b*-values in this study is 5 per cent. Because the method of constant number of events leads to a less reliable spatial resolution in the given case of an irregular event density (Fig. 9), the accuracy of the *b*-values around the outer edges of the cross-sections in Fig. 10 is to be neglected, as well as the *b*-values calculated for the region beneath the cavity. These are artefacts of the method. We did not include these regions into our interpretation. However, comparisons with the method of constant radius showed that the locations of the *b*-value maxima, their spatial dimensions as well as the size of their *b*-values are reliable and highly agreeing. Additionally, *b*-values of several sub-volumes have been determined manually for a comparison with the 3-D distribution and confirmed the previously obtained *b*-values.

The completeness of the catalogue is a major factor for the significance of the *b*-values. It is important to evaluate the influence of gaps in the data records, such as days of maintenance of the network, network saturation due to high event rates, or events that cannot be located due to too few *P*- and *S*-wave onsets. The largest event-station distance in our dataset is 198 m. Especially at these large distances it is likely that the localization criterion of ten triggered stations is sometimes not fulfilled.

For testing the influence of temporal gaps, we analysed the events that occurred in a 3000 m^3 large sub-volume between October 2003 and end of December 2004. The sub-volume produced 9200 AE events during the considered time period and had an overall *b*-value of 1.9 ± 0.02 and a magnitude of completeness of 44 dB. In the following, we took the same subset, but removed all events from each fourth subsequent hour. This lead to the exact same *b*-value and magnitude of completeness as before. As a third test, we took again the original subset, but removed the events that were recorded during all weekends. This reduced the *b*-value only to 1.82 ± 0.02, which is still within our standard deviation of 5 percent, and did again not change the magnitude of completeness.

Considering the fact that the numbers of recorded events within the 3 months time periods are still unusually high compared to other *b*-value studies, we conclude that short temporal gaps in the catalogue do not significantly affect the presented *b*-values.

A systematic shift in location of events of a certain size may also possibly bias the spatial *b*-value patterns (Wiemer, personal communication, 2009). From all the tests we performed (changing time span, changing sample sizes, changing M_c) we would exclude that this is a large effect in our dataset. Although the dataset covers only a small range of magnitudes, limited by the dynamic range of the network, dividing it into 3 months time periods ensures a high enough number of events for calculating reliable *b*-values.

DISCUSSION

Fig. 12 shows a sketch of the local geological features around the investigated area. The sketch relies on geological studies undertaken by the Federal Institute for Geosciences and Natural Resources (BGR). A large block of anhydrite is directly located above the cavity, with a second anhydrite block lying above it to its western side. The surrounding rock mass mainly consists of rock salt. The hatched areas roughly indicate the locations of the *b*-value maxima in the frequency-magnitude distributions (Fig. 10) at depths of about –240 and –280 m, respectively. Considering the geological model, each of these two regions is expected to consist mainly of rock salt.

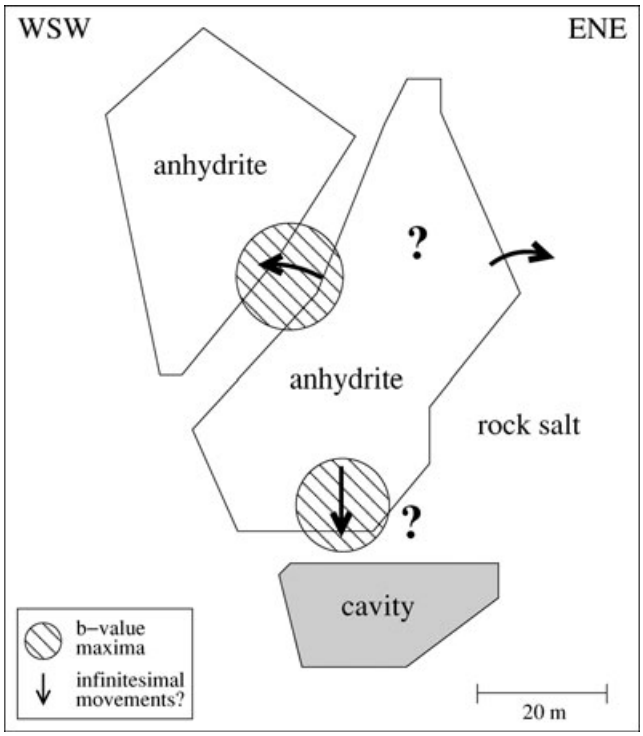

Figure 12. Geological sketch of a vertical cross-section through the area around the investigated rock mass. The sketch has been produced after geological maps from the Federal Institute for Geosciences and Natural Resources (BGR). The hatched areas indicate the locations of the *b*-value maxima (Fig. 10) at depths of about –240 and –280 m, respectively. The errors indicate possible infinitesimal movements of the anhydrite block—however, these remain unclear.

The first one is embedded between the two anhydrite blocks, and the second one is located between the cavity and the anhydrite block. Both regions show transitions between the different materials rock salt and anhydrite. The latter region is also the area that is mostly influenced by the temperature variations during and after backfilling of the cavity, which should make the induced stress largest compared to the other areas within the investigated rock mass. Indeed, we found a high number of events with larger magnitudes in this region. By heating the rock salt directly above the cavity, the anhydrite block above could be stressed as a whole due to increased creeping of the salt and the development of microcracks. It remains unclear if the anhydrite block is stressed as a whole and if it even reacts with infinitesimal movements like tilting or subsidence. More likely is an accumulation of stress at the material boundaries or a re-activation of single existing fissures within the anhydrite block. The transition zones between different materials are the most sensible parts; they only need small stress changes to activate microcracks. This could also explain the high *b*-values at a depth of –240 m, where—according to the geological model—a layer of rock salt is surrounded by anhydrite.

Previous studies undertaken by the BGR showed that different rock types can cause differently sized *b*-values. Away from mining activity, areas in the Morsleben mine that mainly consisted of rock salt regularly led to higher *b*-values than areas of anhydrite (Spies & Eisenblätter 2001a). This is in good agreement with the results obtained by Scholz (1968), since rock salt behaves more ductile than anhydrite.

A comparison of the geological model (Fig. 12) with the frequency-magnitude distributions (Fig. 10) suggests not only that

the maximum *b*-values are located at the transition zones between the different materials, but it can also be noted that the eastern half of the kidney-shaped volume of high *b*-values is in good agreement with shape and size of the anhydrite block directly located above the cavity. Our observations of *b*-value sizes during backfilling and thermal loading are just the opposite as found by the BGR. We found highest *b*-values of up to 3.18 within the anhydrite block and smaller *b*-values in the rock salt. The effect cannot be easily attributed to a different loading of the two rock masses, which are neighbouring each other. It must be noted though, that the geological model is only a rough sketch and the exact size and coordinates of the anhydrite blocks might differ slightly from the location of our *b*-value patterns. However, the sharp contrasts in *b*-values still indicate that structural parameters have indeed controlled the different patterns in *b*.

Assuming that the energy magnitude relation of earthquakes holds for microcracks, *b*-values larger than 1.5 indicate an unstable process, since smaller events would radiate more energy than larger ones. Such a system is in a transient stage and cannot exist for a long time. Indeed, all other observations of anomalous large *b*-values are associated with transient stress loadings (e.g. Warren & Latham 1970; Haycox *et al.* 2005; Hazzard 1998). This indicates that earthquake statistics and *b*-values behave differently during the equilibrium stage of the rock, where stress rate is constant, and during transient stressing. A dependency of earthquake seismicity and swarm activity on the temporal pattern of the applied load has been postulated by Toda *et al.* (2002), when studying the aftershock and swarm activity during a strong magmatic intrusion at Izu Islands (Japan) in 2000. The smoothly changing stress caused swarm activity with high *b*-values, whereas a sudden stress jump controlled the typical mainshock–aftershock behaviour of tectonic earthquakes. Our findings support that seismicity controlling parameters depend on the stressing rate. During periods of constant stressing rate, *b*-values in anhydrite (b_a) and rock salt (b_s) are both at a normal level and $b_a < b_s$. During periods of changing stress rate, *b*-values increase to anomalous high values and $b_a > b_s$.

Can we postulate the different mechanism to rupture cracks in anhydrite and rock salt? During transient loading, ruptures in rock salt apparently grow larger compared to anhydrite ($b_a > b_s$). Rock salt is believed to be more homogeneous than anhydrite, so that newly formed cracks in response to transient loading are not hindered in growth and create larger events. The resistance to crack growth is possibly larger in anhydrite because of the more heterogeneous structure. During periods of constant stress rate (equilibrium stage), a different mechanism is important. The ambient stress has equilibrated, since the number and size of newly formed cracks accommodates the stressing. Ductile flow and visco-plastic stress release is more efficient in rock salt than in anhydrite so that ambient stress is possibly smaller in rock salt, and the likelihood of a large region of high shear stress is reduced; large events in rock salt are more seldom.

Although aspects of the proposed model are qualitatively discussed in many papers before, the conclusions and consequences we draw are of more importance. One should be careful when periods of stationary *b*-values are compared to periods where temporal *b*-value changes occur. This may lead to mis-interpretations. Although spatial differences in changing *b*-values tell us something about the structure and heterogeneity of the rock, the spatial differences in stationary *b*-values indicate more how large the ambient stress is and whether visco-plastic or aseismic stress relaxation is efficient. For instance, during stationary periods, spatial variations in *b*-values indicate differences in ambient stress and where and whether aseismic stress relaxation is efficient. In contrast, during time periods of transients, the spatial variations of *b*-values are additionally controlled by the structure and heterogeneities of the rock.

Is the study of AE in rock salt and anhydrite of relevance to earthquakes? We think it is. The statistical behaviour and general trends resemble the behaviour during volcanic swarms or aftershock sequences of large earthquakes. Although these studies often lack a good statistical basis and unknown loading scenarios, our experiment is ideal with respect to these points. The rate of well-located events was up to 6000 events per day and the analysing period was more than 1 yr. The stress loading was man-made and thus well understood. However, it has to be stated that evaporates like rock salt and anhydrite may behave fracture-mechanically different compared to other sediments or intrusive rocks.

ACKNOWLEDGMENTS

We thank the Federal Institute for Geosciences and Natural Resources for the permission to work with the provided data and to publish this paper. We also thank the GMuG mbH and Drs. Eisenblätter and Manthei for helping with many questions regarding the data and processing. The constructive comments by Stefan Wiemer and an anonymous reviewer are greatly appreciated. We would also like to thank the editor for suggesting the electronic supplements to this paper. The figures were created using GMT (http://gmt.soest.hawaii.edu/) and Matlab (http://www.mathworks.com/).

REFERENCES

Aki, K., 1965. Maximum likelihood estimate of b in the formula log $N = a–bM$ and its confidence limits, *Bull. Earthq. Res. Inst.,* **43,** 237–239.

Amitrano, D., 2003. Brittle–ductile transition and associated seismicity: experimental and numerical studies and relationship with the *b* value, *J. geophys. Res.,* **108**(B1), 2044, doi:10.1029/2001JB000680.

Behlau, J. & Mingerzahn, G., 2001. Geological and tectonic investigations in the former Morsleben salt mine (Germany) as a basis for the safety assessment of a radioactive waste repository, *Eng. Geol.,* **61,** 83–97.

Federal Office for Radiation Protection, 2001. Endlager Morsleben: Das Endlager für radioaktive Abfälle vor der Stilllegung, *Bundesamt für Strahlenschutz (BfS),* http://www.bfs.de/transport/bfs/druck/broschueren/morsleben.html (2009 June 9).

Gutenberg, B. & Richter, C.F., 1949. *Seismicity of the Earth and associated phenomena,* Princeton University Press, Princeton, NJ.

Haycox, J., Pettitt, W. & Young, R.P., 2005. Äspö Pillar Stability Experiment. Acoustic emission and ultrasonic monitoring, SKB Report R-05-09, Swedish Nuclear Fuel and Waste Management Co., Sweden.

Hazzard, J.F., 1998. Numerical modelling of acoustic emissions and dynamic rock behaviour, *PhD thesis*. Keele University, Keele, Staffordshire, UK.

Ishimoto, M. & Iida, K., 1939. Observations sur les seism enregistré par lemicroseismograph construite dernierment (I), *Bull. Earthq. Res. Inst.,* **17,** 443–478.

Kreienmeyer, M., Schmidt, H., Gläß, F. & Mauke, R., 2004. Central part of the Morsleben repository—geomechanical situation before stabilization, in *Proceedings of Disposal Technologies and Concepts (DisTec), International Conference on Radioactive Waste Disposal,* 2004 April 26–28, Berlin.

Mogi, K., 1962. Magnitude-frequency relation for elastic shocks accompanying fractures of various materials and some related problems in earthquakes (2nd Paper), *Bull. Earthq. Res. Inst. Univ. Tokyo,* **40,** 831–853.

Pettitt, W., 1998. Acoustic emission source studies of microcracking in rock, *PhD thesis*. Keele University, Keele, Staffordshire, UK.

Scholz, C.H., 1968. The frequency-magnitude relation of microfracturing in rock and its relation to earthquakes, *Bull. seism. Soc. Am.,* **58,** 399–415.
Schorlemmer, D., Neri, G., Wiemer, S. & Mostaccio, A., 2003. Stability and significance tests for *b*-value anomalies: example from the Tyrrhenian Sea, *Geophys. Res. Lett.,* **30**(16), 1835, doi:10.1029/2003GL017335.
Schorlemmer, D., Wiemer, S. & Wyss, M., 2005. Variations in earthquake-size distribution across different stress regimes, *Nature,* **437,** 539–542.
Spies, T. & Eisenblätter, J., 2001a. Acoustic emission investigation of microcrack generation at geological boundaries, *Eng. Geol.,* **61,** 181–188.
Spies, T. & Eisenblätter, J., 2001b. Acoustic emission monitoring of closely spaced excavations in an underground repository, *J. Acoust. Emission,* **19,** 153–161.
Spies, T., Hesser, J., Eisenblätter, J. & Eilers, G., 2005. Measurements of acoustic emission during backfilling of large excavations, in *Proceedings of the Sixth International Conference on Rock Bursts and Seismicity in Mines (Perth),* pp. 379–383. Australian Centre for Geomechanics, Perth.
Toda, S., Stein, R.S. & Sagiya, T., 2002. Evidence from the AD 2000 Izu islands earthquake swarm that stressing rate governs seismicity, *Nature,* **419,** 58–61.
Urbancic, T.I., Trifu, C.-I., Long, J.M. & Young, R.P., 1992. Space-time correlations of *b* values with stress release, *Pure appl. Geophys.,* **139,** 449–462.
Warren, N.W. & Latham, G.V., 1970. An experimental study of thermally induced microfracturing and its relation to volcanic seismicity, *J. geophys. Res.,* **75,** 4455–4464.
Wiemer, S., 2001. A software package to analyze seismicity: ZMAP, *Seism. Res. Lett.,* **72,** 373–382.
Wiemer, S. & McNutt, S.R., 1997. Variations in the frequency-magnitude distribution with depth in two volcanic areas: Mount St. Helens, Washington, and Mt. Spurr, Alaska, *Geophys. Res. Lett.,* **24,** 189–192.
Wiemer, S. & Wyss, M., 2000. Minimum magnitude of completeness reporting in earthquake catalogs: examples from Alaska, the Western United States, and Japan, *Bull. seism. Soc. Am.,* **90,** 859–869.
Woessner, J. & Wiemer, S., 2005. Assessing the quality of earthquake catalogues: estimating the magnitude of completeness and its uncertainty, *Bull. seism. Soc. Am.,* **95**(2), 684–698, doi:10.1785/0120040007.
Wyss, M., 1973. Towards a physical understanding of the earthquake frequency distribution, *Geophys. J. R. astr. Soc.*, **31,** 341–359.

SUPPORTING INFORMATION

Additional Supporting Information may be found in the online version of this article:

Supplement S1. Two supplementary figures; spatial variation of M_c, and 3-D views of Fig. 10.

Please note: Wiley-Blackwell are not responsible for the content or functionality of any supporting materials supplied by the authors. Any queries (other than missing material) should be directed to the corresponding author for the article.